RSC Advances

ROYAL SOCIETY OF CHEMISTRY

www.rsc.org/advances

ARTICLE TYPE www.rsc.org/xxxxxx | XXXXXXXX

Shape-controlled synthesis of $MnCO_3$ nanostructures and their applications in supercapacitors

Ning Zhang[a], Jianmin Ma[b], Qian Li[a], Jia Li[a] and Dickon H. L. Ng[a]

Received (in XXX, XXX) Xth XXXXXXXXX 200X, Accepted Xth XXXXXXXXX 200X
First published on the web Xth XXXXXXXXX 200X
DOI: 10.1039/b000000x

$MnCO_3$ nanospheres and nanocubes have been successfully synthesized by a facile precipitation method utilizing ethylene glycol. When these $MnCO_3$ samples were employed as electrodes in the pseudocapacitor with aqueous $NaClO_4$ electrolyte, they exhibited excellent supercapacitor characteristics. The $MnCO_3$ nanospheres showed a specific capacitance of 129 Fg^{-1} at 0.15 Ag^{-1}, while the nanocube electrode had a specific capacitance of 91 Fg^{-1} at the same current density. The as-prepared $MnCO_3$ electrode materials had a high retention of 87% and 92% after 1000 cycles at 0.3 Ag^{-1}, indicating a high-rate electrochemical cycling life. This study had highlighted the promissing prospects of $MnCO_3$ as a novel electrode material used for supercapacitors.

1. Introduction

Supercapacitors (SCs), refer to a family of electrochemical capacitors which bridge the gap between conventional capacitors and rechargeable batteries.[1-3] They have many advantages compared with traditional capacitor, such as high specific power, high available capacitance values per unit volume, long cycle life with adaptable to a wide range of temperature, high electrical efficiency and environmental protection.[4-6] As a result, SCs would be potentially applied in various fields such as portable electronic devices and hybrid electric vehicles.[7-9] SCs can be classified into two categories, electric double-layer capacitors (EDLCs) and pseudocapacitors.[10] The EDLCs accumulate charges at the electrode/electrolyte interface,[11, 12] while fast and reversible faradic processes would take place in the pseudocapacitors.[13] Because of highly reversible faradic reaction, the pseudocapacitors have higher specific capacitance and energy density than EDLCs with many potential applications.[14-16] Thus, novel electrode materials are often pursued in the study of high-performance pseudocapacitors.

Ruthenium oxide (RuO_2) was considered to be one of the most advantageous candidates as the electrode material for SCs due to its high capacitance, reversible charge-discharge feature as well as superior electrical conductivity.[17-19] However, the high cost of ruthenium, the low porosity and toxic nature of the RuO_2 limit its popularity.[20-22] Recently, much effort has been focused on transitional metal compounds containing nickel, cobalt and manganese with different morphologies. Mai et al. have synthesized $MnMoO_4/CoMoO_4$ heterostructured nanowires with good electrochemical properties.[23] Qu and co-workers designed and synthesized a novel three-dimensional frame architecture of cobalt oxide nanostructure, which exhibits high comprehensive electrochemical performance.[24] Hercule et al. created interconnected nanorods-nanoflakes $Li_2Co_2(MoO_4)_3$ structure serves as electroactive material for SCs and it delivers a high rate capability and long cycle stability.[25] These transitional metal compounds with high specific surface area have superior electrochemical performance, low cost and non-toxic characters had been widely used as electrode materials for SCs.[23-31] Although some transitional metal oxides, hydroxides and even sulphides are being used as electrode materials for supercapacitors, only a few products with metal carbonates are reported.[32, 33] This work explores the feasibility of using manganese carbonate as a new kind of promising raw materials for supercapacitors, since it is environmental friendly, and can be easily fabricated with excellent capacitance performance.

Here we presented a facile co-precipitation method assisted with ethylene glycol for synthesizing shape-controlled $MnCO_3$ nanostructures.[34, 35] Electrochemcial results indicated that the specific capacitance of $MnCO_3$ nanospheres (NSs) and nanocubes (NCs) are 129 Fg^{-1} and 91 Fg^{-1} at the current density of 0.15 Ag^{-1}, respectively. They also exhibited excellent charge-discharge cycling stability. Only 13% and 8% of the values of the original specific capacitance were lost after 1000 cycles at current density of 0.3 Ag^{-1} for the $MnCO_3$-NSs and NCs, respectively.

2. Experimental

Manganese sulfate monohydrate ($MnSO_4 \cdot H_2O$; from Tianjin Hengxing Chemical Reagent Co. Ltd), and sodium bicarbonate (NaHCO;from Tianjin Hengxing Chemical Reagent Co. Ltd) were received and directly used. 0.015M of $MnSO_4$ solution in a mixture of water and ethylene glycol (EG) were under vigorous agitation before 0.15M of $NaHCO_3$ solution was added. The $MnCO_3$-NSs and $MnCO_3$-NCs were then obtained by adjusting the concentrations of water and EG with different volume ratios of 30% and 50% *v*/*v*, respectively. The mixed solution of $MnSO_4$ and $NaHCO_3$ was stirred for 4 hours at room temperature to get the turbid liquid. The obtained precipitates were filtered and washed with deionized water and ethanol before drying at 60 °C for 12 hours.

Structure, composition and morphology of the as-synthesized samples were examined by X-ray diffraction (XRD) using a Rigaku (RU300) diffractometer with Cu Kα radiation (λ = 0.1540598 nm); scanning electron microscopy (SEM) using a Quanta F400 FE-SEM at an accelerating

voltage of 20 kV; electron transmission microscopy using a Tecnai 20 FEG TEM equipped with an energy-dispersive X-ray (EDX) spectrometer at 120 kV. The Brunauer−Emmmett−Teller (BET) and Barrett-Joyner-Halenda (BJH) analyses were also conducted by using the Gemini VII 2390.

The electrochemical characterization of the as-prepared electrode materials included cyclic voltammetry (CV), galvanostatic charge/discharge (GCD), cycling stability and electrochemical impedance spectroscopy (EIS). All of these measurements were carried out at room temperature by using a CHI760 electrochemical working station with a three-electrode system. During the test, an 0.1M $NaClO_4$ aqueous electrolyte solution was used. A platinum foil served as counter electrode, while a saturated calomel electrode (SCE) served as the reference electrode. The working electrode material was prepared by mixing the as-synthesized $MnCO_3$, carbon black and PVDF (as binder) in a weight ratio of 70:20:10. The prepared electrode material was pasted directly onto a nickel foam current collector (1.0 cm×1.0 cm). The formed collector was pressed under 10 MPa and dired at 60°C under vacuum for 12 hours.

3. Results and discussion

3.1 Characterization

Fig.1 shows the XRD patterns of as-synthesized samples ($MnCO_3$-NSs and $MnCO_3$-NCs). All the diffraction peaks are indexed to the phase of $MnCO_3$ (JCPDS card No.44-1472) and no irrelevant peaks are detected in the XRD pattern which confirms $MnCO_3$ nanostructures are pure.

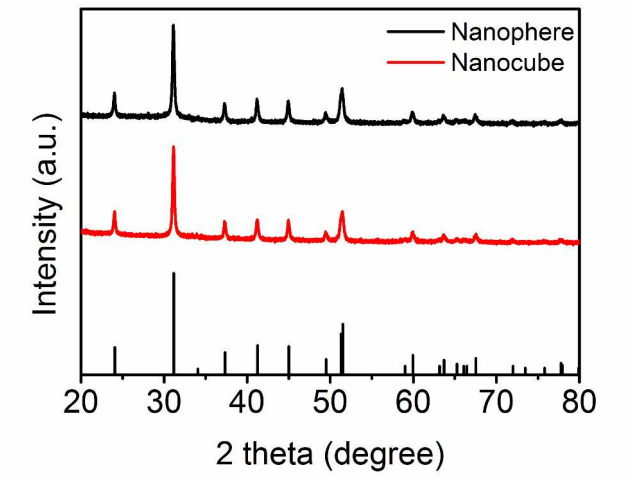

Fig. 1 XRD patterns of the as-synthesized samples ($MnCO_3$-NSs and $MnCO_3$-NCsprepared with 30% and 50% of EG,respectively).

The SEM images of $MnCO_3$-NSs and $MnCO_3$-NCs structures are shown in Fig.2 (a-d). We can find that the well monodispersed spheres in Fig. 2 (a,b) and cubes in Fig. 2 (c,d) under different magnifications. The diameter of as-prepared $MnCO_3$-NSs is ranging from 600 to 800nm. While the $MnCO_3$-NCs are smaller, ranging from 500 to 600nm in size. From the high magnification images Fig. 2 (b,d), we observed that the $MnCO_3$-NSs and NCs structures were formed by the piling up of layers nanoflakes, which indicating that the nanostructures apparently formed by depositting of the smaller aggregates onto larger ones.[36] Our synthetic process also provides a possible way to tune the particle morphology. It is reported that anions of the reactants obviously play an important role in determining the final morphology of the carbonates products.[37, 38] For instance, the existing SO_4^{2-} ions in solution tend to facilitate the formation of spherical structure.[39] On the other hand, the ethylene glycol organic additive has the suitable co-ordination capability to interact with the metal ions and changes their activity in the solution.[40] As a result, the morphology of $MnCO_3$ nanostructures can be controlled by adding different anions and ethylene glycol organic additive.

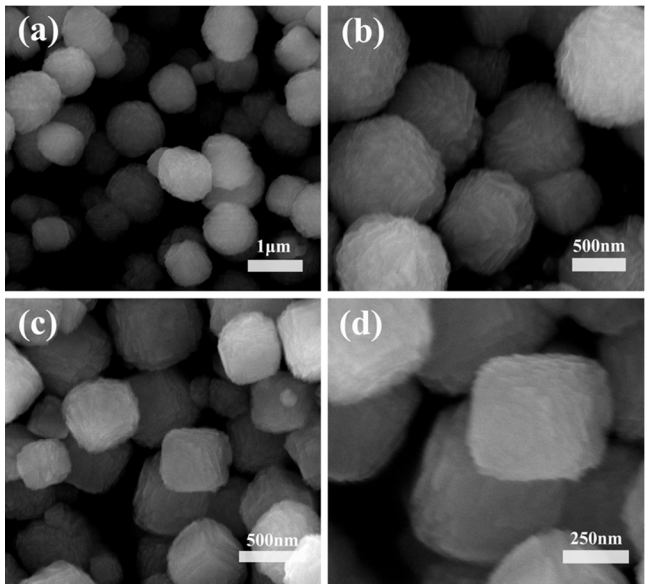

Fig. 2 (a, c) Low- and (b, d) high-magnification SEM images of $MnCO_3$-NSs and $MnCO_3$-NCs samples.

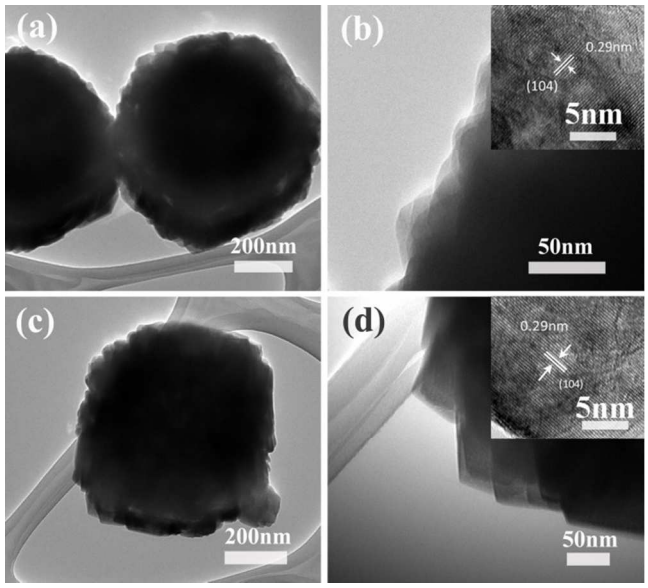

Fig. 3 TEM images of $MnCO_3$-NSs (a, b) and $MnCO_3$-NCs(c, d), respectively. The insert of b and d are the high resolution TEM images of the two samples.

In order to illutstrate the morphology and architecture of $MnCO_3$ in detail, typical TEM images of $MnCO_3$-NSs and $MnCO_3$-NCs are obtained and shown in Fig. 3 (a-d). In detail, Fig. 3 (a, b) and (c, d) show the sphere and cube which consists of numerous interconnected nanoflakes, which forming the continuous monodisperse structures. Moreover, the HR-TEM images of the NSs (insert of Fig. 3b) and for the NCs (insert of Fig. 3d) reveal their crystalline character of the as-prepared $MnCO_3$ phase. The well defined fringes can be seen on both NSs and NCs samples; and the interplanar spacing is about 0.29 nm, which corresponds to the (104) plane of the $MnCO_3$.

The nitrogen adsorption/desorption isotherms and the BJH pore size distribution curves of $MnCO_3$-NSs and $MnCO_3$-NCs are shown in Fig. 4. According to the IUPAC classification scheme, it is evident that the obtained isotherms belong to type IV. The specific surface area of $MnCO_3$-NSs is 28 m^2 g^{-1}, which is higher than that of the $MnCO_3$-NCs with 21 m^2 g^{-1}. The nitrogen sorption isotherms and Barrett-Joyner-Halenda (BJH) pore size distributions of these samples are ranged from 2 to 200nm.

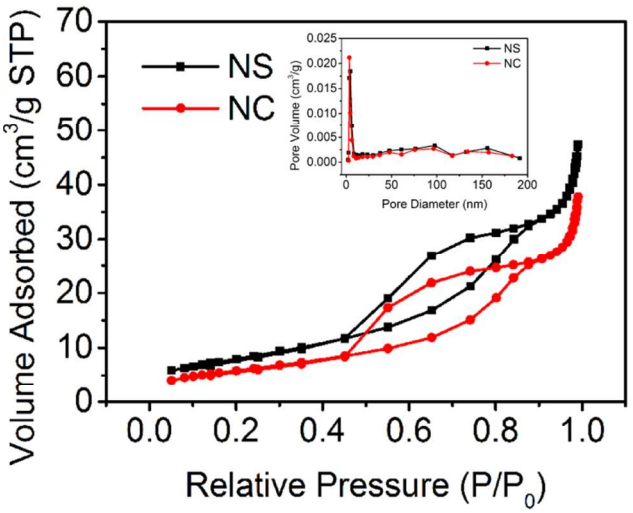

Fig. 4 Nitrogen adsorption/desorption isotherms of $MnCO_3$-NSs and $MnCO_3$-NCs. Insert are the corresponding pore size distribution curves of the $MnCO_3$-NSs and $MnCO_3$-NCs.

3.2 Electrochemical measurements

A three-electrode system was used to characterized the electrochemical properties of the as-synthesized $MnCO_3$-NSs and $MnCO_3$-NCs in their application as electrode materials in the 0.1M $NaClO_4$ aqueous electrolyte. Fig. 5 (a,b) shown the cyclic voltammetry (CV) results of the as-prepared $MnCO_3$-NSs and NCs electrodes in the voltage potential between 0 and 0.9V under various sweep rates from 2 to 20 mV/s. It was obvious that the CV curves showed rectangular-like shapes under different scan rates, indicating good charge propagation within the electrodes and exhibiting characteristics for supercapacitors with excellent capacitance behavior. Typically, CV curves in Fig. 5(a,b) for both $MnCO_3$-NSs and $MnCO_3$-NCs tended to deviate from ideal rectangular shape at high scan rate of 20mV/s due to the sluggish ion incorporation into the electrode material. The CV measurements were also performed in a 6 M KOH aqueous electrolyte. The results are shown in Fig. 5c and 5d, where the curves exhibit pairs of pseudo redox peaks under different scan rates from 2 to 20mV/s. The results are consistent with some previous result reported. [32]

To further evaluate the electrochemical properties of the $MnCO_3$-NSs and $MnCO_3$-NCs, we had measured the galvanostatic charge/discharge behaviors for both kinds of electrodes in 0.1M $NaClO_4$ aqueous electrolyte, which are shown in Fig. 5e and 5f. It was noted that the discharge curves for both the $MnCO_3$-NSs and NCs samples could be divided into three regions. In the first region, region I, due to the internal resistance of electrode material, there exhibited a sudden drop in current at the start of the discharge. In region II, a linear variation of the time dependence of the potential indicated the double-layer capacitance behavior, which was probably caused by the charge separation which was taking place between the electrode and electrolyte interface. In region III, a slope variation of the time dependence of the potential indicated a typical pseudo-capacitance behavior, which was a result of the electrochemical adsorption/desorption or redox reaction taking place at the interface between electrode and electrolyte.[41] The specific capacitance value of the $MnCO_3$ nanostructure could be calculated by :

$$C_m = \frac{I\Delta t}{m\Delta V},$$

where C_m is the specific capacitance, I is the constant charge/discharge current, Δt is the discharge time, m is the total mass of electrode material and ΔV is the potential difference of the electrode. In our samples, the specific capacitance contribution from the nickel foam current collector was ignored. It was justifiable because its capacitance was determined to be 0.1 F/g under the current density of 0.1 A/g in a 0.1M $NaClO_4$ aqueous electrolyte, too small to be effective. Fig. 5g shows the specific capacitance values of $MnCO_3$-NSs and $MnCO_3$-NCs obtained under different charge/discharge current density from 0.15 Ag^{-1} to 2 Ag^{-1}. At the low current density 0.15 Ag^{-1}, the specific capacitance of the as-synthesized $MnCO_3$-NSs electrode exhibited the specific capacitance approximating to 129 Fg^{-1}, which was higher than that previously reported.[32] As shown in Fig. 5g, the specific capacitance of $MnCO_3$-NSs electrode was larger than that of the $MnCO_3$-NCs electrode. The reason for such difference was owing to the diverse specific surface areas of these two kinds of electordes, which could be evaluated and confirmed by the BET results in Fig. 4. The BET surface area of $MnCO_3$-NSs was found to be 28 m^2g^{-1} which was larger than those in $MnCO_3$-NCs having the value of 21 m^2 g^{-1}.

In order to estimate the stability of the as-synthesized $MnCO_3$ electrodes, we had also measured the cycling performance of the electrode materials in 0.1M $NaClO_4$ aqueous electrolyte at a current density of 0.3 Ag^{-1} and the results were revealed in Fig. 5h. After 1000 cycles, the capacitance of the $MnCO_3$-NSs remained at 87% and that of $MnCO_3$-NCs electrode remained at 92% of the original value.

This demonstrated an excellent long-term stability of the as-synthesized materials as the electrodes for supercapacitors.

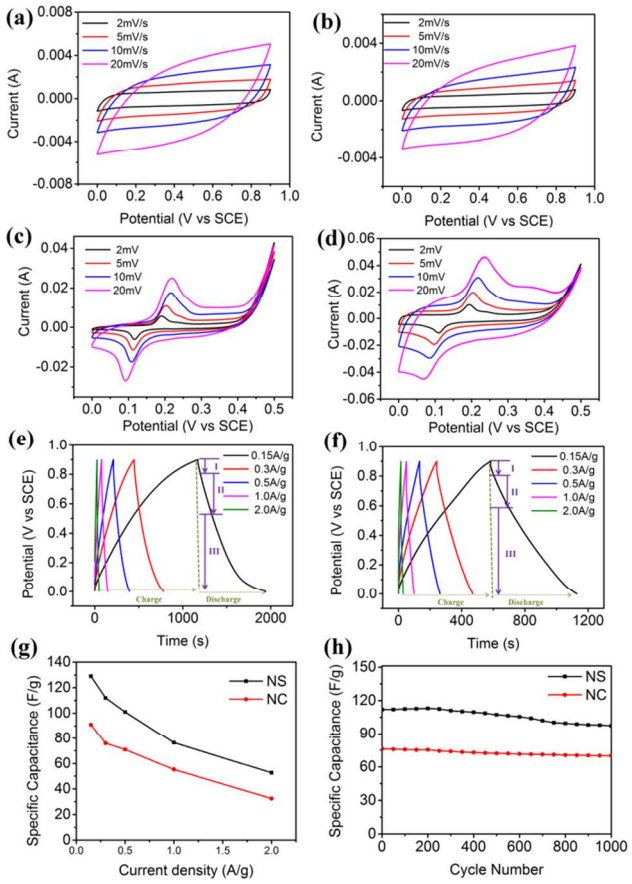

Fig. 5 (a-b) CV curves of $MnCO_3$-NSs and $MnCO_3$-NCs electrodes in 0.1M $NaClO_4$ aqueous electrolyte under different scan rates at voltage potentials between 0 and 0.9V, (c-d) CV curves of $MnCO_3$-NSs and $MnCO_3$-NCs electrodes in 6M KOH aqueous electrolyte under different scan rates, (e-f) charge/discharge curves of NSs and NCs in 0.1M $NaClO_4$ aqueous electrolyte, (g) rate performance of the two types of electrodes, (h) cycling performance of electrodes at the current density of 0.3 Ag^{-1}.

The electrochemical performances of these two kinds of electrodes were further confirmed by the electrochemical impedance spectroscopy (EIS) measurements performed in a 0.1M $NaClO_4$ aqueous electrolyte over the frequency range 0.01–100,000Hz. The results are shown on Fig. 6. The EIS data were analyzed using the Nyquist plots. For both spectroscopies, a semicircle in the high-frequency region and a straight line at low frequency region could be observed. An equivalent circuit consisting of a bulk solution resistance R_s, a charge-transfer R_{ct}, a pseudocapacitive element C_p from the redox process, and a constant phase element (CPE) to account for the double-layer capacitance figure was inserted in Fig. 6.[24] The initial non-zero intercept in high frequency region at the beginning of the semicircle was identical in both the curves which was resulted from the bulk solution resistance R_s, while the semicircle represented the charge transport resistance R_{ct}. After calculated by the Zview software, the solution resistance R_s of these two kinds of electrodes ($MnCO_3$-NSs and NCs) was determined to be 16.86 Ω and 21.6 Ω, while the charge-transfer resistance R_{ct} of the $MnCO_3$-NSs was 131.8Ω, which was smaller than 216.6 Ω of the $MnCO_3$-NCs. Evidently, this also indicated that the lower resistance of $MnCO_3$-NSs resulted in a better electrochemical performance. It was also mentioned that, owing to the relatively large charge-transfer resistances of both $MnCO_3$-NSs and $MnCO_3$-NCs compared with other kinds of electrode materials, the specific capacitances of $MnCO_3$-NSs and $MnCO_3$-NCs would not be as good under high current density situation.[42, 43]

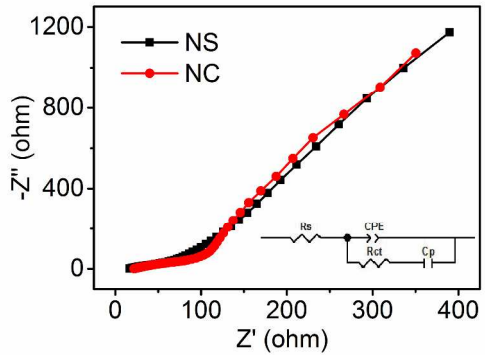

Fig. 6 The electrochemical impedance spectra (EIS) of the electrodes at room temperature; The insert shows the equivalent circuit for the electrochemical impedance spectra.

4. Conclusions

In summary, we have successfully designed and synthesized the monodispersed $MnCO_3$ nanosphere and nanocube samples by a facile co-precipitation method. The structure and morphology of the as-synthesized material were characterized by XRD, SEM, TEM and BET measurements. The electrochemical characterizations of $MnCO_3$ nanostructures, including cyclic voltammetry, galvanostatic charge/discharge and cycling stability were measured by a three-electrodes system. The $MnCO_3$-NSs and NCs nanostructures exhibited well supercapacitor characteristics, relatively high specific capacitance and excellent long-term stability. The as-obtained $MnCO_3$ nanomaterials are expected to be one of the promising electrode materials for supercapacitors.

Acknowledgement

This work was supported by the HKSAR Government RGC-GRF Grant (CUHK14303914) and by the Direct Grant (Project Code: 4053076) from the Faculty of Science, The Chinese University of Hong Kong.

Notes and references

[a] *Department of Physics, The Chinese University of Hong Kong, Hong Kong; E-mail: dng@phy.cuhk.edu.hk*

[b] Key Laboratory for Micro-/Nano-Optoelectronic Devices, School of Physics and Electronics, Hunan University, Changsha 410082, China

See DOI: 10.1039/b000000x/

1. H. Y. Lee and J. B. Goodenough, *J. Solid State Chem.*, 1999, **144**, 220-223.
2. P. Simon and Y. Gogotsi, *Nat Mater*, 2008, **7**, 845-854.

3. Y. Wang, Z. Shi, Y. Huang, Y. Ma, C. Wang, M. Chen and Y. Chen, *J. Phys. Chem. C*, 2009, **113**, 13103-13107.
4. L. Wei and G. Yushin, *Nano Energy*, 2012, **1**, 552-565.
5. Y. Zhu, S. Murali, M. D. Stoller, K. J. Ganesh, W. Cai, P. J. Ferreira, A. Pirkle, R. M. Wallace, K. A. Cychosz, M. Thommes, D. Su, E. A. Stach and R. S. Ruoff, *Science*, 2011, **332**, 1537-1541.
6. L. Nyholm, G. Nystrom, A. Mihranyan and M. Stromme, *Adv. Mater.*, 2011, **23**, 3751-3769.
7. P. Simon and Y. Gogotsi, *Acc. Chem. Res.*, 2012, **46**, 1094-1103.
8. Y. Zhang, H. Feng, X. Wu, L. Wang, A. Zhang, T. Xia, H. Dong, X. Li and L. Zhang, *Int. J. Hydrogen Energy*, 2009, **34**, 4889-4899.
9. R. A. Fisher, M. R. Watt and W. Jud Ready, *ECS J. Solid State SC.*, 2013, **2**, M3170-M3177.
10. M. F. De Volder, S. H. Tawfick, R. H. Baughman and A. J. Hart, *Science*, 2013, **339**, 535-539.
11. G. Wang, L. Zhang and J. Zhang, *Chem Soc Rev*, 2012, **41**, 797-828.
12. Y. Zhai, Y. Dou, D. Zhao, P. F. Fulvio, R. T. Mayes and S. Dai, *Adv. Mater.*, 2011, **23**, 4828-4850.
13. H. B. Li, M. H. Yu, F. X. Wang, P. Liu, Y. Liang, J. Xiao, C. X. Wang, Y. X. Tong and G. W. Yang, *Nat Commun*, 2013, **4**, 1894.
14. J.-K. Chang and W.-T. Tsai, *J. Electrochem. Soc.*, 2003, **150**, A1333.
15. Q. Li, X. F. Lu, H. Xu, Y. X. Tong and G. R. Li, *ACS Appl Mater Interfaces*, 2014, **6**, 2726-2733.
16. X. Wang, Z. Li, J. Shi and Y. Yu, *Chem Rev*, 2014, DOI: 10.1021/cr400633s.
17. C.-C. Hu, K.-H. Chang, M.-C. Lin and Y.-T. Wu, *Nano Letters*, 2006, **6**, 2690-2695.
18. P. Soudan, J. Gaudet, D. Guay, D. Bélanger and R. Schulz, *Chem. Mater.*, 2002, **14**, 1210-1215.
19. I. L. Chen, T.-Y. Chen, C.-C. Hu and C.-H. Lee, *J. Mater. Chem. A*, 2013, **1**, 2039.
20. D. Han, P. Xu, X. Jing, J. Wang, P. Yang, Q. Shen, J. Liu, D. Song, Z. Gao and M. Zhang, *J. Power Sources*, 2013, **235**, 45-53.
21. Y. Li, H. Fu, Y. Zhang, Z. Wang and X. Li, *J. Phys. Chem. C*, 2014, **118**, 6604-6611.
22. X. Xia, J. Tu, Y. Mai, R. Chen, X. Wang, C. Gu and X. Zhao, *Chemistry*, 2011, **17**, 10898-10905.
23. L. Q. Mai, F. Yang, Y. L. Zhao, X. Xu, L. Xu and Y. Z. Luo, *Nat Commun*, 2011, **2**, 381.
24. L. Qu, Y. Zhao, A. M. Khan, C. Han, K. M. Hercule, M. Yan, X. Liu, W. Chen, D. Wang, Z. Cai, W. Xu, K. Zhao, X. Zheng and L. Mai, *Nano Lett*, 2015, **15**, 2037-2044.
25. K. M. Hercule, Q. Wei, O. K. Asare, L. Qu, A. M. Khan, M. Yan, C. Du, W. Chen and L. Mai, *Advanced Energy Materials*, 2015, **5**, n/a-n/a.
26. Y. Yang, G. Ruan, C. Xiang, G. Wang and J. M. Tour, *J Am Chem Soc*, 2014, **136**, 6187-6190.
27. C. H. Tang, X. Yin and H. Gong, *ACS Appl Mater Interfaces*, 2013, **5**, 10574-10582.
28. Z. Tang, C.-h. Tang and H. Gong, *Adv. Funct. Mater.*, 2012, **22**, 1272-1278.
29. C. Xiang, M. Li, M. Zhi, A. Manivannan and N. Wu, *J. Power Sources*, 2013, **226**, 65-70.
30. G. Yu, L. Hu, N. Liu, H. Wang, M. Vosgueritchian, Y. Yang, Y. Cui and Z. Bao, *Nano Lett*, 2011, **11**, 4438-4442.
31. X. Zhang, X. Sun, Y. Chen, D. Zhang and Y. Ma, *Mater. Lett.*, 2012, **68**, 336-339.
32. S. Devaraj, H. Y. Liu and P. Balaya, *J. Mater. Chem. A*, 2014, **2**, 4276.
33. J. Yuan, J. Zhu, H. Bi, Z. Zhang, S. Chen, S. Liang and X. Wang, *RSC Adv.*, 2013, **3**, 4400.
34. H. K. Lee, D. Sakemi, R. Selyanchyn, C. G. Lee and S. W. Lee, *ACS Appl Mater Interfaces*, 2014, **6**, 57-64.
35. A. A. Antipov, D. Shchukin, Y. Fedutik, A. I. Petrov, G. B. Sukhorukov and H. Möhwald, *Colloid Surface. A*, 2003, **224**, 175-183.
36. C. K. King'ondu, A. Iyer, E. C. Njagi, N. Opembe, H. Genuino, H. Huang, R. A. Ristau and S. L. Suib, *J Am Chem Soc*, 2011, **133**, 4186-4189.
37. X. Xiao, J. Lu and Y. Li, *Nano Research*, 2010, **3**, 733-737.
38. J. Fei, Y. Cui, X. Yan, Y. Yang, K. Wang and J. Li, *ACS Nano*, 2009, **3**, 3714-3718.
39. A. Cao and A. Manthiram, *Phys Chem Chem Phys*, 2012, DOI: 10.1039/c2cp40209b.
40. Y. Sun and Y. Xia, *Science*, 2002, **298**, 2176-2179.
41. D. P. Dubal, V. J. Fulari and C. D. Lokhande, *Micropor. Mesopor. Mat*, 2012, **151**, 511-516.
42. H. Pang, J. Deng, J. Du, S. Li, J. Li, Y. Ma, J. Zhang and J. Chen, *Dalton Trans*, 2012, **41**, 10175-10181.
43. H. Pang, S. Wang, G. Li, Y. Ma, J. Li, X. Li, L. Zhang, J. Zhang and H. Zheng, *J. Mater. Chem. A*, 2013, **1**, 5053.